Application of two-dimensional sandwich structure supported Pt single-atom catalyst in photocatalytic hydrogen evolution: first principle

Yanshuai Li[1], Shizhi Dong[1,2,*], Bingshuai Zhu[1], Ruichuan Li[1], Wenlong Shang[1], Linghui Chen[1], Jinyu Zhang[1], Zhilong Zhao[1], Lin Guo[2]

1.College of Materials Science and Engineering, Liaoning Technical University, Fuxin, 123000, China;

2.School of Chemistry and Environment, Beihang University, Beijing, 100191, China

Corresponding author: Shizhi Dong

E-mail: xiaodong8125@163.com

Abstract: The preparation of hydrogen by photocatalytic principle is an important subject in the future energy direction. This article intends to design the catalytic structure of a crystalline (amorphous) TiO_2/two-dimensional MoS_2 sandwich structure supporting a single-atom, and explore the effect of this special structure on the photocatalytic reaction.Calculating the effective mass, electrostatic potential, light absorption spectrum and other related properties by DFT method, the analysis shows that the sandwich structure catalyst has good carrier transfer ability and electron-hole separation ability. Except for the Pt@Amorphousr-TiO_2/MoS_2 sandwich structure single-atom catalyst, which only has an excellent effect on the oxygen evolution of water, the rest of the interlayer catalysts have the two characteristics of photocatalytic hydrogen evolution and oxygen evolution.The new catalyst designed in this paper has innovative design ideas and high-efficiency research and development value.

Key words: Heterostructure; First principle; Work function; Photocatalysis; Amorphous materials

1 Introduction

In few years, mitigation of energy and environmental issues is a must for sustainable development in China and the world[1]. Although some progress has been made in the development of new renewable energy sources such as hydro, tidal and wind power, the development of these sources is particularly constrained by geographical constraints, which prevent their further application. Hydrogen is also one of these clean and renewable sources of energy, which providing 2.5 times more energy per unit of mass than traditional fossil fuels. Unfortunately, hydrogen producting is now mainly from non-renewable sources at the present stage, therefore it is a fundamental task that developing a clean, renewable solution to obtain hydrogen. Nowadays, semiconductor based water splitting photocatalysis has attacted great interests on account of its importance to solve the energy crisis and environmental pollution[2-3].

2D van der Waals(vdWs)Heterojunction materials are kind of new semiconductor materials designed by energy band engineering, which have good size design, large interface contact area, reveal better the catalytic advantages of each component, and can quickly promote the separation and transfer of photogenerated charges, and expand the diversity of photocatalyst system[4]. Recently, 2D metal oxynitrides and oxysulfides have emerged as novel photocatalysts, in which the valence band is composed of N-2P and S-3P States, and the energy is higher than O-2P state, resulting in the narrowing of the band gap, which can better provide the active reaction center and effectively inhibit the recombination of photogenerated electrons and holes[5]. In general, the band gap (E_g) of 2D materials will increase by the decreasing of thicknesses, and with the upward movement of conduction band bottom (CBM) and downward movement of valence band top (VBM)[6]. For example, the E_g of bulk TiO_2 is about 3.2 eV, CBM and

VBM are - 0.5V and 2.7V, respectively(Compared with standard hydrogen electrode, pH = 7, similarly hereinafter). However, for two-dimensional TiO_2, its CBM moves up by 0.12V, while VBM decreases by 0.48V, and E_g will increase at the same time, which leads to its excellent electronic and optical properties, so it is widely used in photocatalysis[7-8].

Gu *et al.* using interfacial assembly method has prepared TiO_2 / g-C_3N_4 photocatalyst with the second kind of heterostructure[9], Under UV visible light irradiation, both g-C_3N_4 and TiO_2 can be excited by photon energy higher than their band gap. Due to the unique ultra-thin 2D face-to-face contact characteristics, the distance between g-C_3N_4 and TiO_2 is very short, resulting in the photocatalytic hydrogen evolution rate of 18,200 μmol $g^{-1}h^{-1}$. After that,Zhong and coworkers prepared a new type of g-C_3N_4/TiO_2 compound material[10], The effect of photocatalytic hydrogen evolution is enhanced under visible light. Due to its excellent mechanical and electronic properties, MoS_2 will play an important role in the design and development of catalysts in the future. Therefore, Huaming Li *et al.* developed MoS_2 / g-C_3N_4 two-dimensional heterojunction photocatalyst to remove environmental pollutants[11-12]. Then, the photocatalysis of TiO_2 / MoS_2 heterostructure has been developed[13]. Yuan *et al.* have loaded two-dimensional molybdenum disulfide nanosheets on the surface of two-dimensional titanium dioxide nanosheets[14]. By loading the optimal amount of 0.50wt% molybdenum disulfide as the co-catalyst, the photocatalytic ability of TiO_2 to produce H_2 was significantly improved. However, for heterostructure or sandwich structure, the theoretical understanding of the system is still not perfect, the internal relationship of interlayer coupling is not clear, and the research of defect environment on the electron hole recombination degree is not enough, which has affected the rapid development of photocatalyst.

For example, electron correlation in amorphous heterostructures. In recent years, amorphous materials have emerged in the field of electrocatalysis and showed excellent catalytic activity[15]. Band tail absorption often occurs in amorphous materials[16], Moreover, there are a large number of unsaturated sites and defects, which can sometimes be called the active sites of the reaction. At the same time, some shallow traps can repeatedly capture and release photogenerated electrons / holes, and then affect the migration time of photogenerated charges. Some amorphous transition metal compounds can be used as cocatalysts, and their photocatalytic activity is not inferior to that of noble metals[[17]. If the amorphous material is compounded with the crystalline material, the advantages of the amorphous material can be embodied, the active sites can be increased, and the negative effect of the lattice mismatch between the interfaces can be eliminated[18].

After Tao Zhang Academician proposed the concept of "single-atom catalysts(SACs)", Pt noble metal SACs with low cost, high selectivity and high active site has become an important member of green catalysts[19-20]. However, clusters are more likely to occur on the surface energy of single atom, and Ostwald ripening is more likely to occur with the decrease of particle size[21]. Noble metal chemical catalyst is an important raw material for the production of

metal catalyst because of its excellent comprehensive chemical application performance, such as waterproof, acid-base corrosion resistance, high temperature resistance and oxidation resistance. From the perspective of environmental protection and economy, the most important thing is the innovative design of functional support for noble metal single-atom catalyst.

Based on the above, in this paper, the crystal (amorphous) two-dimensional structure rutile TiO_2(r-TiO_2)/single atom Pt supported on crystalline MoS_2 sandwich structure is designed (It is difficult to form high quality vdws heterojunction due to the influence of layer spacing), to constructing novel functionalized single-atom photocatalysts. First of all, is to fill the gap of the new type of catalyst with sandwich structure, the other is to reveal the structure-activity of the catalyst for the defect sandwich structure. The electronic properties and optical absorptivity of the photocatalyst were analyzed by density functional theory. It is hoped that the research ideas and basis can be provided for the design of the functional support of the single atom photocatalyst.

2 Method of calculation

In this paper, we use the Materials studio quantum computing software CASTEP module to calculate the related properties. The exchange correlation energy is calculated by using the Perdew-Burke-Ernzerhof (PBE) functional under the generalized gradient approximation (GGA), and the r-TiO_2(110) and MoS_2(0001) are selected the surface, and the amorphous r-TiO_2 model is formed by rapid cooling under the NVT ensemble. Table 1 shows the optimized structure parameters of rutile TiO_2 and MoS_2. Compared with the literature, the surface parameters and sandwich structure parameters of rutile TiO_2 and MoS_2 are shown in Table 1 within a reasonable range.

Table 1 Structural parameters for material optimization

Materials	a(Å)	b(Å)	c(Å)	
r-TiO_2	4.62	4.56	2.98	This work
r-TiO_2	4.56	4.56	2.95	**[22]**
Amorphous r-TiO_2(110)	4.65	4.51	-	This work
MoS_2	3.18	3.14	4.92	This work
MoS_2	3.22	3.22	4.86	**[23]**
r-TiO_2(110)	5.92	6.45	-	This work
MoS_2(0001)	6.33	5.49	-	This work
r-TiO_2(110)/MoS_2(0001)	6,13	6.00	-	This work

Then, the interlayer structure was constructed, and Pt single atom was loaded on the surface of titanium oxide. The interlayer spacing was controlled at about 5 Å, the precision of truncation radius was set to Fine, and the truncation energy was 570 eV. The K-point grid in Brillouin zone is 4 × 4 × 1. The strong Coulomb exchange interaction between electrons of transition metal d-level is considered. The electronic structure is analyzed by the OTFG ultra-soft pseudopotential calculation of CASTEP module, and the vdWs force is corrected by Tkatchenko-Scheffler(TS) dispersion correction. In order to avoid the interference of periodic arrangement and eliminate the interaction between atoms, the thickness of vacuum layer is selected as 10 Å. In this work, the geometric

structure is optimized after the force and energy standards reach 0.1 eV/Å and 10^{-5} eV respectively, and the maximum displacement is 0.01 Å. At this time, the total energy of the system is the lowest, which ensures that the model is closer to the actual crystal structure(Fig. 1).

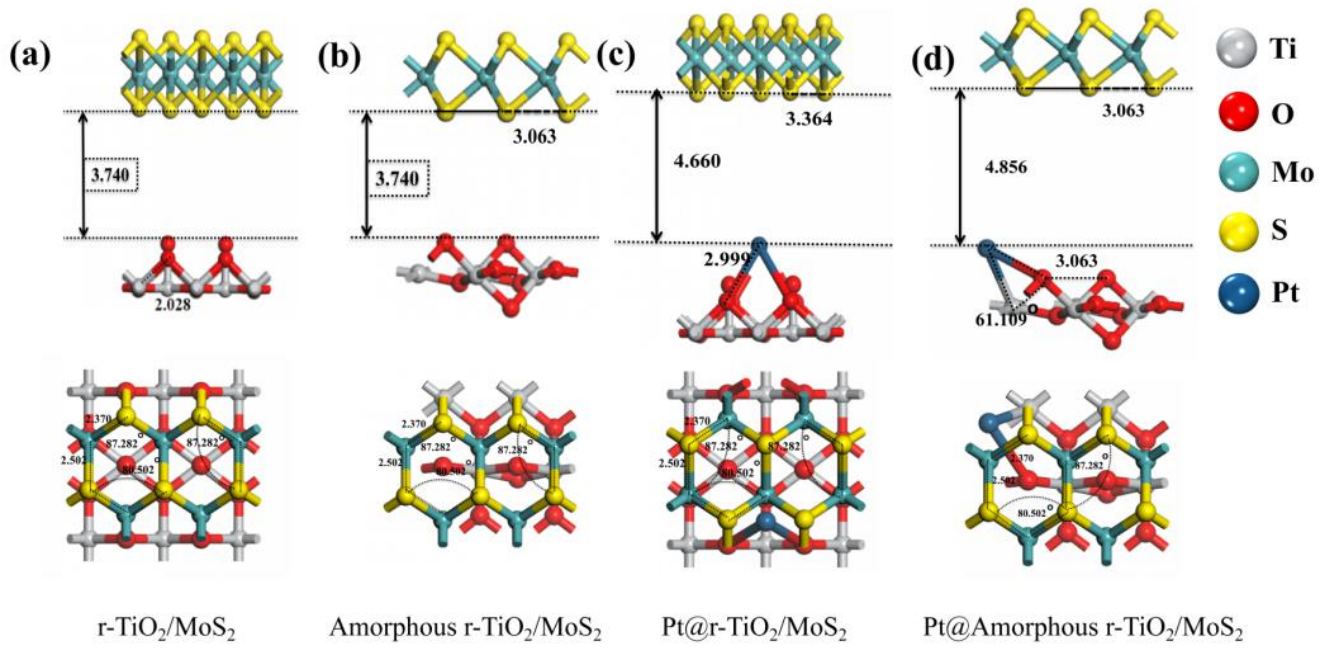

Fig. 1 structure diagram of sandwich structure catalyst

3 Interpretation of result

3.1 Stability analysis of catalyst

For testing the stability of amorphous r-TiO_2 (110) surface , in the NVT ensemble, the total step size is 5ps, a total of 2500 steps, as shown in Fig.2, the energy fluctuates around -3999.5803 Ha, It shows that the structure of amorphous r-TiO_2 is stable.

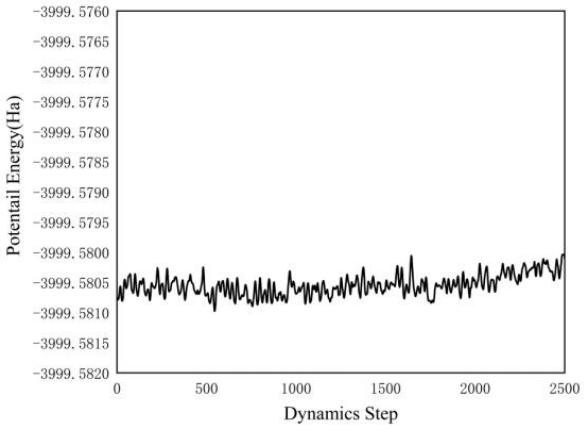

Fig.2 Calculation of Molecular Dynamics Stability of Amorphous r-TiO_2

After ensuring the stability, we calculated the formation energy of monolayer structure and crystalline (amorphous) r- TiO_2 / MoS_2 sandwich structure(as shown in Table 2),The formation energy is calculated as follows

$$\Delta E_{xA\cdot yB} = x \times \Delta E_A + y \times \Delta E_B - \Delta E_{total}$$

The results show that both the monolayer structure and the sandwich structure can exist stably, and then Pt atoms

are adsorbed on the sandwich structure, The adsorption energy formula is as follows

$$\Delta E_{chem} = E_{Pd\ \ on\ \ M} - E_M - E_{Pd}$$

The adsorption energy is less than -0.5eV, which indicates that the atoms have a stable chemical adsorption. It can also be seen that the adsorption of Pt atoms on amorphous r- TiO_2/ MoS_2 sandwich structure is more stable, which indicates that the high electron concentration on the surface of amorphous material plays a role.

Table 2 Properties of sandwich structure catalysts

	binding energy(eV)	adsorption energy(eV)	active mass(m_0)	Band gap(eV)
r-TiO_2(110)	-0.07	-	1.27	4.56
Amorphous r-TiO_2(110)	-0.84	-	1.43	2.70
MoS_2(001)	-0.08	-	2.25	1.92
r-TiO_2/MoS_2	-1.78	-	1.94	1.49
Amorphous r-TiO_2/MoS_2	-1.70	-	0.30	1.12
Pt@r-TiO_2/MoS_2	-	-3.43	0.54	0.78
Pt@Amorphous r-TiO_2/MoS_2	-	-5.32	0.25	1.22

3.2 Analysis of electronic performance of catalyst

After the stability of the system is satisfied, we discuss the electronic properties of the catalyst. The band gap of single layer r- TiO_2 is 4.56 eV, which is close to that of 4.70 eV reported in literature[24],The band gap of MoS_2 is 2.10 eV, which is almost the same as 2.0 eV in the literature[25]. Fig.3 shows the energy band diagram of the sandwich structure catalyst. Generally speaking, the four structures have semiconductor characteristics, and the band gap is within 0.78 eV-1.49 eV. Fig.3 (a) and (d) are indirect band gaps, which indicate the existence of phonon scattering, which will hinder the effective carrier migration. The effective mass of the sandwich structure catalyst is given in Table 2. It is well known that the effective mass is inversely proportional to the carrier mobility. Therefore, the carrier mobility of r- TiO_2 / MoS_2 catalyst is the smallest, the difference is that Pt@Amorphous r- TiO_2 / MoS_2 catalyst has the largest carrier mobility. The reason may be that there is a strong electronic structure on the surface of the amorphous structure, which shows excellent transmission performance with single atom Pd loading.

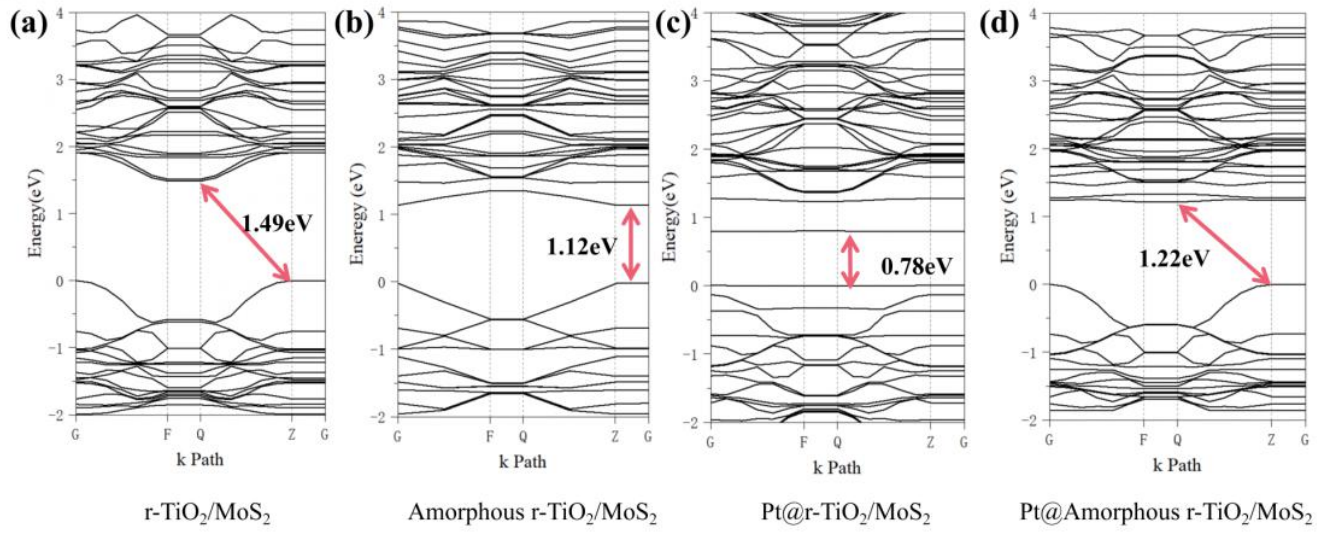

Fig. 3 band diagram of sandwich structure catalyst

Fig.3 (b) and (c) show the direct band gap, but Fig.3 (c) shows the direct band gap Pt@r-TiO_2/MoS_2 fluctuation near the Fermi level of the catalyst is small, and the degree of electron delocalization is low. Therefore, even if the band gap is small, the degree of electron migration decreases. On the whole, (b) ~ (d) catalysts have higher carrier mobility.

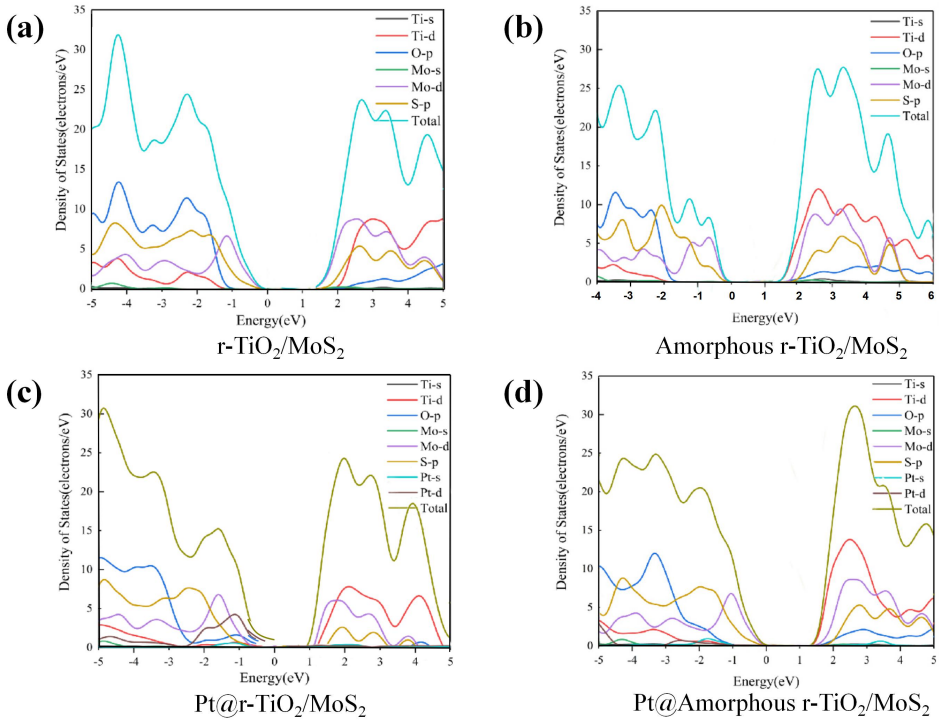

Fig. 4 density of states of catalyst with sandwich structure

Combined with the partial wave density of states of the catalyst (Fig. 4), we can clearly see the orbital contribution of atoms near Fermi level. Compare Fig. 4 (a) with (b), the S-s and Mo-d orbitals on the valence band side play a major role in carrier transport, while the Ti-d orbitals on the conduction band side provide electron contribution. Therefore, the interlayer interface has good transmission characteristics. At the same time, the atomic orbitals of Ti and Mo cross and the bonding strength increases, which indicates that the system is stable. Fig.4 (c) ~ (d) shows the

contribution of Pt atoms in the catalyst, the Fermi level of the Pt-5d orbital in the Pt@r-TiO_2/MoS_2 model, can provide more transport electrons near the valence band, which can provide more coordination sites for the reaction. The Pt-5d orbital of Pt@Amorphous r-TiO_2/MoS_2 is basically near the inner of the valence band, which indicates that the interlayer catalysts has a better binding degree at this time. In the follow-up reaction simulation, it will stably adhere to the carrier and effectively catalyze the reaction.

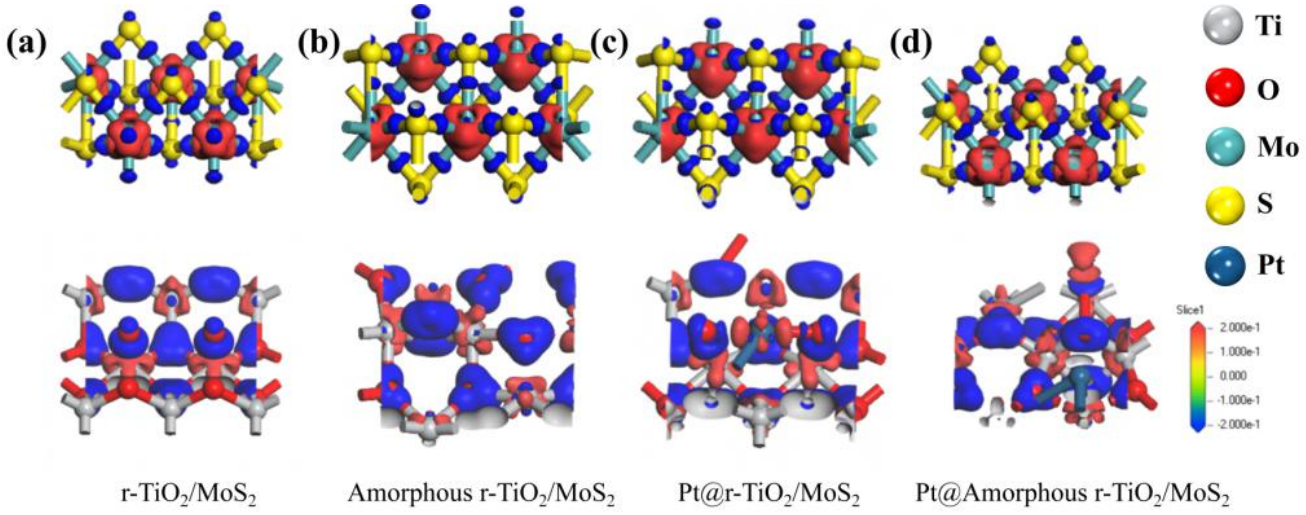

Fig. 5 differential charge density diagram of sandwich structure catalyst

Next, we analyze the electron distribution of the catalyst. Fig.5 is the schematic diagram of the differential charge density of the catalyst. Red indicates the increase of the electron concentration, and blue indicates the decrease of the electron concentration. It is found that there is a good electron transport property between the layers of the sandwich structure. After loading single atom, there is a strong electron gain and loss near the Pt atom, which indicates that the d orbital of Pt participates in the interface electron bonding. The density of electron cloud between Pt atom and Ti atom overlaps, in the Pt@r-TiO_2/MoS_2 model, the electron density near Pt increases, while the electron density near O atom decreases, there's a directed electron migration.In the interlayer catalyst of Pt@Amorphous r-TiO_2/MoS_2, the electron concentration near Pt atom decreases and the electron moves to Ti atom. The reason may be that the unsaturated coordination environment on the amorphous surface is favorable for the electron movement on the material surface.

Combined with the results of atomic population and bond length population (as shown in Fig. 6 and Table 3), the bonding situation can be more clear. In layout analysis, positive indicates bonding, negative indicates anti bonding or no bonding (according to the key length). It can be seen that there are both ionic bond and covalent bond in two-dimensional MoS_2, and the bonding degree of two-dimensional titanium oxide is higher than that of covalent bond. The bond length between atoms is also relatively standard, and there is no structural distortion due to the interlayer structure. In the structure of Pt@r-TiO_2/MoS_2 catalyst, there is bonding between Ti-O and anti bonding between O-Pt. We can see that the Ti-Pt and O-Pt of the Pt@Amorphous r-TiO_2/MoS_2 are bonding, and the binding stability is better,

which can be used to analyze the density of states.

Table 3 atomic and chemical bond populations of sandwich catalysts

	r-TiO_2/MoS_2	Amorphous r-TiO_2/MoS_2	Pt@r-TiO_2/MoS_2	Pt@Amorphous r-TiO_2/MoS_2
Mo(1)	0.12e	0.14e	0.15e	0.15e
Mo(2)	0.14e	0.15e	0.15e	0.16e
S(1)	-0.12e	-0.12e	-0.11e	-0.13e
S(2)	-0.12e	-0.18e	-0.13e	-0.13e
Ti(1)	1.10e	1.18e	1.12e	1.12e
Ti(2)	1.35e	1.24e	1.35e	1.36e
O(1)	-0.74e	-0.74e	-0.67e	-0.66e
O(2)	0.39e	-0.62e	-0.49e	-0.61e
Pt	-	-	0.31e	-0.19e
Mo-S	0.44(2.39Å)	0.46(2.38Å)	0.44(2.39Å)	0.44(2.79Å)
Ti-O	0.94(1.61Å)	0.43(1.82Å)	0.79(1.74Å)	0.50(1.82Å)
Ti-Pt	-	-	0.27(2.86Å)	0.31(2.44Å)
O-Pt	-	-	-0.14(2.81Å)	0.29(2.61Å)

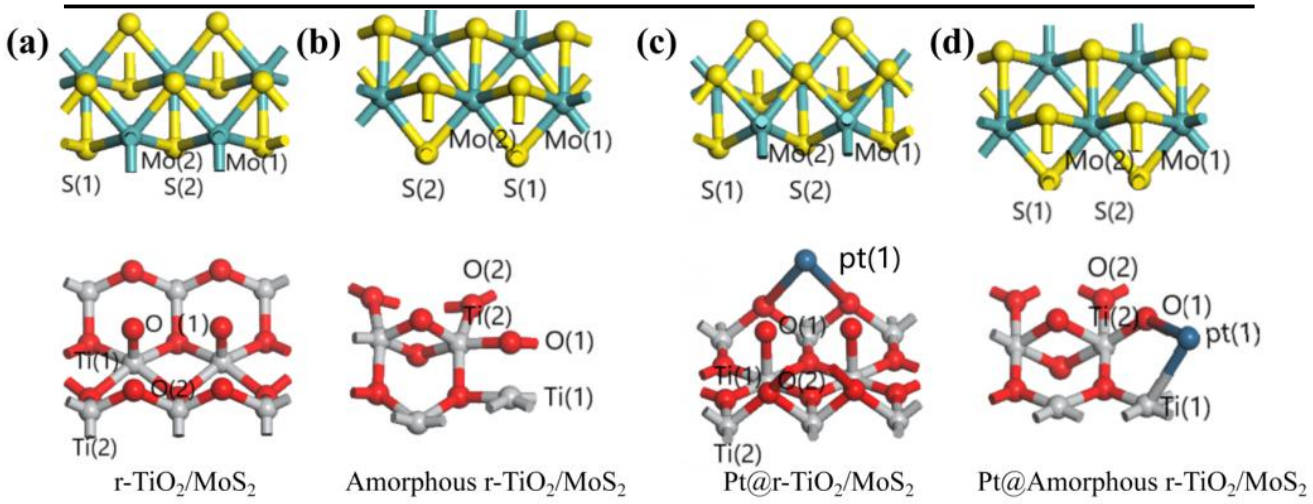

Fig. 6 population atomic number mark of sandwich structure

In addition, we explain the activity of the catalyst from the point of view of the energy overcome by electron migration. The work function is defined as the minimum energy required for electrons to escape from Fermi level to vacuum, which can well reflect the transition ability of outer electrons. The calculation formula of work function is $\varphi = E_{Vac}—E_F$,, where E_{Vac} and E_F are the energies of vacuum level and Fermi level respectively[26]. As shown in Fig.7, the work function of the single-layer material is relatively large, while the work function of amorphous r-TiO_2 is small because the defect structure on the surface has weak binding ability to electrons, resulting in low work function. However, after the formation of the sandwich structure, the electrons on the amorphous surface have limited migration, so the work function of the composite system increases slightly.

Noble metals can also be used as cocatalysts to reduce the over potential of photocatalysis. In addition, due to the local surface plasmon resonance (LSPR) effect of noble metals, the visible light absorption capacity of the catalyst system is enhanced. Therefore, when we look at Fig.7 (f) ~ (g), we will find that the work function of the corresponding system decreases by 0.7 eV and 1.84 eV, respectively, so the electron transition surface is easier. After

the formation of the composite system, the work function is relatively low and the binding energy of the material surface to electrons is low, which can promote the escape of electrons from the material surface and enhance the activity of reactive oxygen species (ROS). Therefore, the material with low work function has a lower activation energy barrier, which makes it possible to use low-energy near-infrared light for photocatalytic reaction.

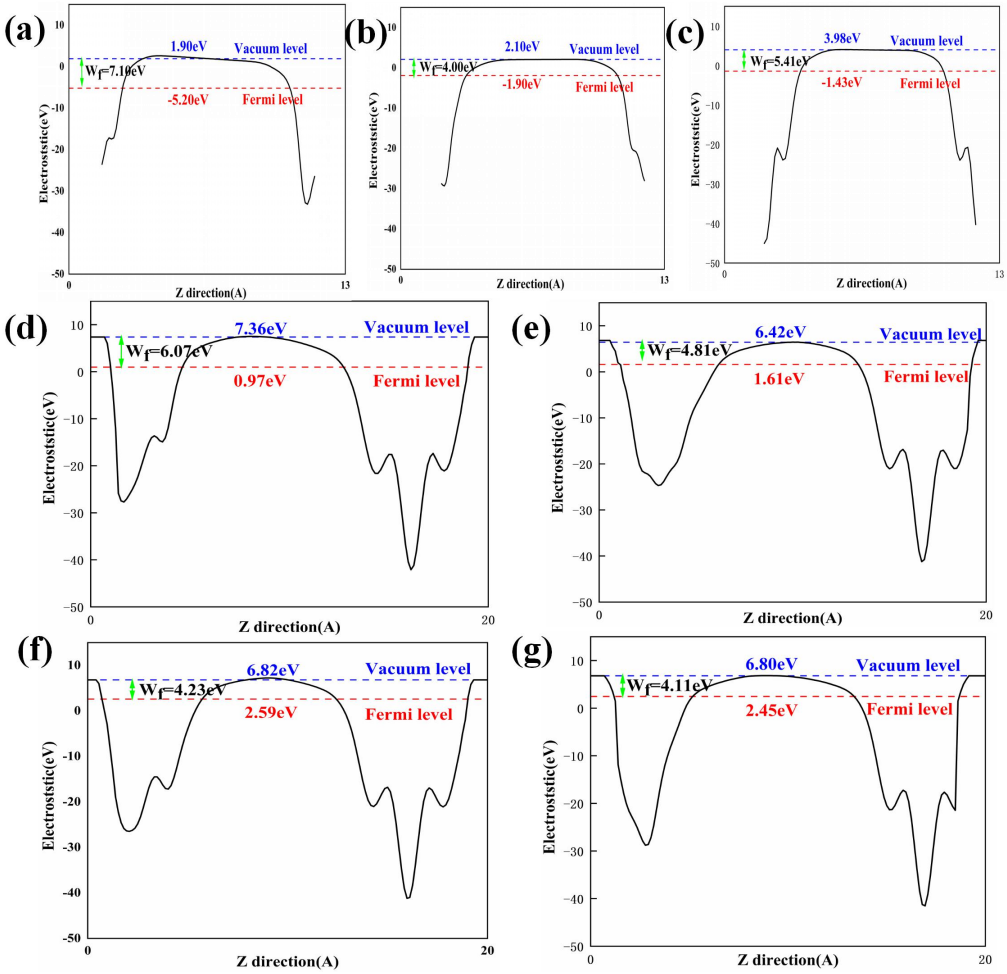

Fig .7 Electrostatic potential and work function of two-dimensional materials and sandwich catalysts; (a) r-TiO_2(110); (b) Amorphous r-TiO_2(110); (c) MoS_2(0001); (d) r-TiO_2(110)/MoS_2(0001); (e) Amorphousr-TiO_2(110)/MoS_2(0001); (f) Pt@r-TiO_2(110)/MoS_2(0001); (g) Pt@Amorphousr-TiO_2(110)/MoS_2(0001)

3.3 Photocatalytic analysis of catalysts

Most of the photocatalysts are limited by the light absorption range or the recombination rate of photo generated carriers. Therefore, in the research of photocatalysis, people have been committed to solving two core problems: 1) expanding the light absorption range of photocatalyst; 2) To improve the separation efficiency of photogenerated carriers. In the last part, the carrier migration ability was introduced in detail. Next, the light absorption ability of the sandwich structure catalyst and its feasibility in photolysis of water were described.

According to the definition of Kramers-Kronig dispersion relation and direct transition probability, the optical constants such as absorption coefficient can be derived:

$$I(\omega)=\frac{\sqrt{2}\omega}{c}\left[\sqrt{\varepsilon_1^2(\omega)+\varepsilon_2^2(\omega)}-\varepsilon_1(\omega)\right]^{1/2}$$

ω is frequency, $\mathcal{E}_1(\omega)$is Real part permittivity, $\mathcal{E}_2(\omega)$is Imaginary part permittivity, When the photon energy reaches the energy gap range, the semiconductor can produce the light electron coupling effect, which can excite the electron transition between the valence band and conduction band. Fig.8 shows the optical absorption spectrum image of sandwich catalysts and monolayer structure. The optical absorption rate of monolayer crystalline and amorphous r-TiO_2 is very low. When the sandwich structure is formed with MoS_2, it can be found that the optical absorption coefficient has been significantly improved. The absorption coefficient of r-TiO_2/MoS_2 sandwich structure catalyst is very close to that of Yang Yang *et al.*[27]. Next, Pt@r-TiO_2/$MoS_2$and Pt@Amorphousr-TiO_2/MoS_2 have the best optical absorption coefficient. We can conclude that the addition of noble metals can promote the photocatalytic activity. According to the report of Peng *et al.*[28], the absorption coefficient of the material with $10^5 cm^{-1}$ light absorption coefficient is equivalent to that of silicon, which can be used as an efficient light absorption material in solar cells and other optoelectronic devices. The performance of this paper is better than that of Man Yao and Jinlong Yang[29-30], therefore, the single atom photocatalysts with sandwich structure has obvious advantages in expanding the light absorption range.

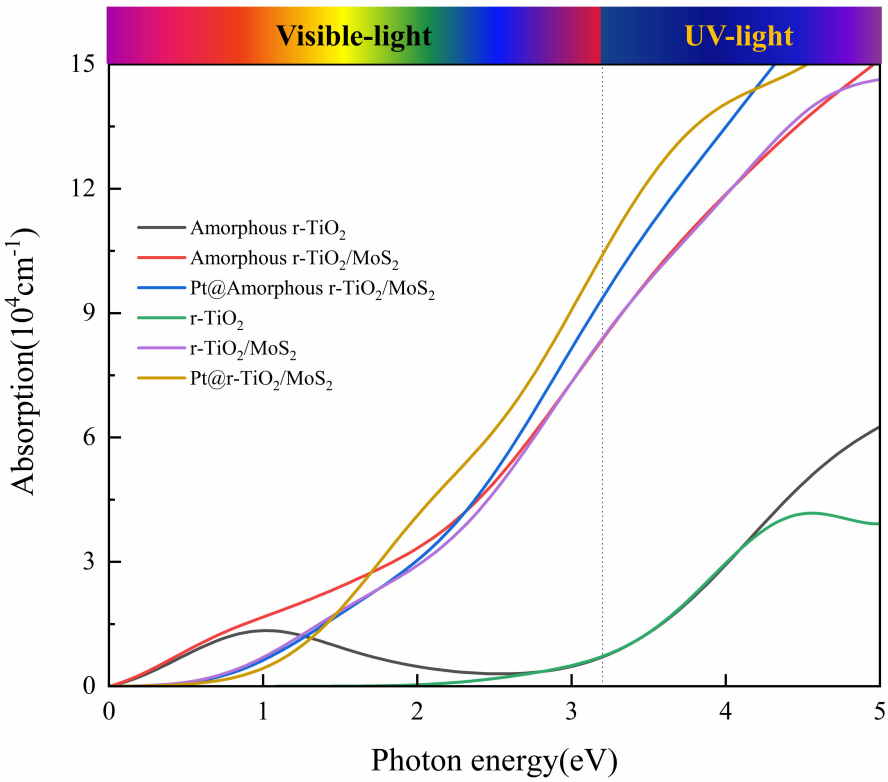

Fig .8 Spectroscopic absorption spectra of two-dimensional materials and sandwich structure catalysts

In order to further analyze the photocatalytic ability of the catalyst. In general, referring to the redox potential of the standard hydrogen electrode, the positions of the corresponding materials conduction band minimum(CBM) and valence band maximum (VBM) can be given by the equation:

$$E_{CB} = \chi - 0.5E_g$$

$$E_{VB} = E_{CB} + E_g$$

CB and VB represent the redox potential at the bottom of conduction band and the top of valence band, respectively, and E_e is the energy of free electron to hydrogen atom (4.5eV), χ Represents the electronegativity of a material. It can be obtained by calculating the geometric mean of the Millikan electronegativity of each atom. The formula is as follows[31]

$$\chi = \left[\chi(A)^a \chi(B)^b\right]^{1/a+b}$$

χ(A) and χ(B) are the electronegativity of two kinds of atoms, a and b are the number of atoms. The photocatalytic hydrolysis mechanism of heterogeneous structure catalyst is shown in Fig.9, which clearly shows that the sandwich structure catalysts has good electron hole separation ability. Under visible light irradiation, it is very possible to realize the transmission of the photoelectric e^- generated at the excited VBM to the CBM by fully absorbing the energy larger than the band gap of the two separated parts. At the same time, the same number of h^+ photons as e^- are generated at the CBM and transferred to the VBM.

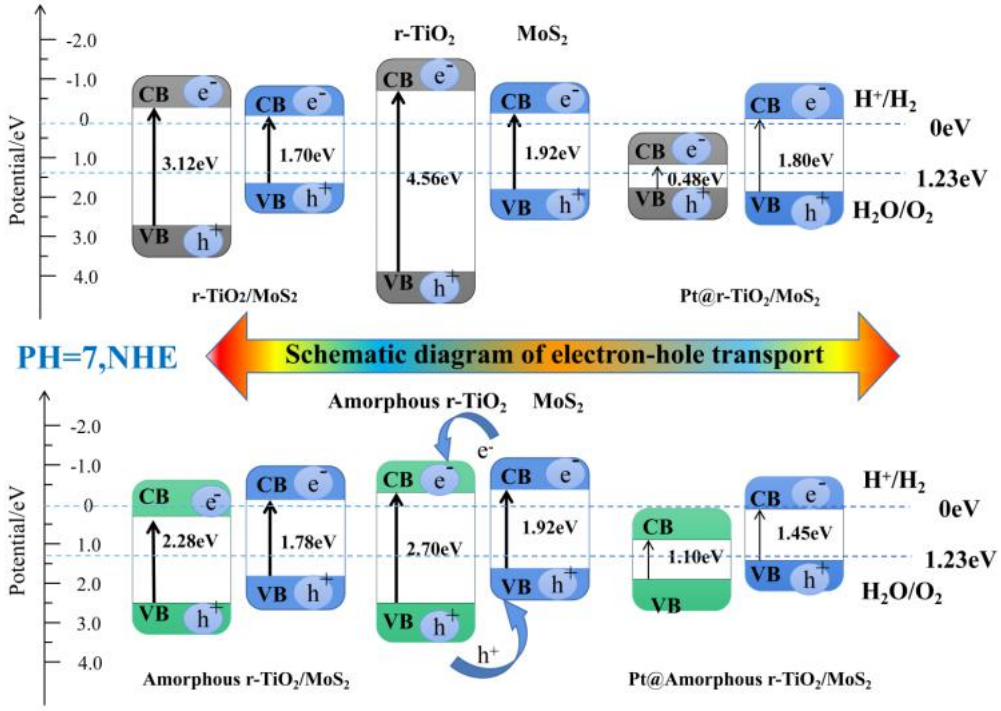

Fig.9 Schematic diagram of carrier migration and separation in sandwich structure photocatalyst

In r-TiO_2 / MoS_2 structure, electrons and holes are transported from TiO_2 to MoS_2 at the same time, and there is no good electron migration ability. However, the band gap of the composite is more than 1.23eV, so the photocatalytic decomposition of water can still be carried out. Amorphousr-TiO_2 / MoS_2 is similar to the second type heterojunction, which can effectively promote the separation of photo excited electron hole pairs. Under the action of conduction band offset (CBO) and valence band offset (VBO), the residual e^- produced in MoS_2 is induced to transfer to CB of r-TiO_2,

while the h^+ accumulated in r-TiO_2, is transferred to VB of MoS_2. The two catalysts were supported by Pt atoms to form a Z-type semiconductor heterostructure. The electrons on the CB of r-TiO_2 are directly combined with the VB holes of MoS_2. In the photocatalytic reaction, the VB holes on r-TiO_2 transport the CB electrons of MoS_2, so they have more excellent electron migration ability.

However, under the influence of the surface defects of amorphous r-TiO_2, the sandwich structure of single-atom catalyst does not have the ability of water desorption of hydrogen. We know that redox reaction can be realized in two independent parts. Therefore, Pt@Amorphousr-TiO_2/MoS_2 catalyst has a bright future in photocatalytic water precipitation of O_2, H_2O_2 and O_3. These products have strong oxidation ability and can directly oxidize many pollutants, which indicates that the development of this new type of photocatalyst is of great significance.

4 Conclusion

This paper presents an innovative design of crystal(amorphous) two-dimensional r-TiO_2/ crystalline MoS_2 sandwich-structured supported single-atom catalysts. And the important application of this system in photocatalysis was described by first principles method. From the point of view of stability, we discussed the electronic properties of the four sandwich structures and the ability of photocatalytic water splitting. The internal electric field formed by the sandwich structure reduces the recombination degree of e^-/h^+ and has good carrier mobility. The reasonable band gap structure makes the intercalated catalyst have higher optical absorption coefficient and lower work function. The Pt@Amorphous-TiO_2/MoS_2 structure of the catalyst has good oxygen evolution characteristics, and the other three structures have comprehensive catalytic effect of water cracking photocatalyst. This design opens up a new way, shows its great application value in the field of hydrogen production, and provides effective guidance for the experiment.

Reference

[1] Dresselhaus, M. S., & Thomas, I. L.. Alternative energy technologies. ***Nature***, 2001, 414(6861), 332-337.

[2] Chen, X., Shen, S., Guo, L., & Mao, S. S.. Semiconductor-based photocatalytic hydrogen generation. ***Chemical Reviews,*** 2010, 110(11), 6503-6570.

[3] Moniz, S. J. A., Shevlin, S. A., Martin, D. J., Guo, Z. X., & Tang, J.. Visible-light driven heterojunction photocatalysts for water splitting - a critical review. ***Energy & Environmental Science***, 2015, 8(3), 731-759.

[4] Gao, M., Chen, L., Zhang, Z., Sun, X., & Zhang, S.. Interface engineering of the Ni $(OH)_2$ – Ni_3N nanoarray heterostructure for the alkaline hydrogen evolution reaction. ***Journal of Materials Chemistry A***, 2018, 6(3), 833-836.

[5] Moriya, Y., Takata, T., & Domen, K. Recent progress in the development of (oxy) nitride photocatalysts for water splitting under visible-light irradiation. ***Coordination Chemistry Reviews***, 2013, 257(13-14), 1957-1969.

[6] Sakai, N., Ebina, Y., Takada, K., & Sasaki, T. (2004). Electronic band structure of titania semiconductor nanosheets revealed by electrochemical and photoelectrochemical studies. ***Journal of the American Chemical Society***, 126(18), 5851-5858.

[7] Wu, Y., Liu, Z., Li, Y., Chen, J., Zhu, X., & Na, P.. Construction of 2D-2D TiO_2 nanosheet/layered WS2 heterojunctions with enhanced visible-light-responsive photocatalytic activity. ***Chinese Journal of Catalysis***, 2019, 40(1), 60-69.

[8] Yuan, L., Weng, B., Colmenares, J. C., Sun, Y., & Xu, Y. J.. Multichannel charge transfer and mechanistic insight in metal decorated 2D-2D Bi_2WO_6-TiO_2 cascade with enhanced photocatalytic performance. ***Small***, 2017, 13(48), 1702253.

[9] Gu W., Lu F., Wang C., *et al.* Face-to-face interfacial assembly of ultrathin g-C3N4 and anatase TiO_2 nanosheets for enhanced solar photocatalytic activity. ***ACS Appl Mater Interfaces***, 2017, 9: 28674 – 28684142.

[10] Zhong R., Zhang Z., Yi H., *et al.* Covalently bonded 2D/2D O-g-C_3N_4/TiO_2 heterojunction for enhanced visible-light photo catalytic hydrogen evolution. ***Appl Catal B-Environ,*** 2018, 237: 1130–1138.

[11] Li J, Liu E, Ma Y, *et al.* Synthesis of MoS_2/g-C_3N_4 nanosheets as 2D heterojunction photocatalysts with enhanced visible light activity. ***Appl Surf Sci***, 2016, 364: 694–702.

[12] Yan J, Chen Z, Ji H, *et al.* Construction of a 2D graphene-like MoS_2/C_3N_4 heterojunction with enhanced visible-light photocatalytic activity and photoelectrochemical activity. ***Chem Eur J,*** 2016, 22: 4764–4773

[13] Wang, W., Zhu, S., Cao, Y., Tao, Y., Li, X., & Pan, D., *et al*. Edge‐enriched ultrathin mos2 embedded yolk-shell TiO_2 with boosted charge transfer for superior photocatalytic H_2 evolution. ***Advanced Functional Materials***, 2019, 29(36), 1901958.1-1901958.10.

[14] Yuan YJ, Ye ZJ, Lu HW, *et al.* Constructing anatase TiO_2 nanosheets with exposed (001) facets/layered MoS_2 two-dimensional nanojunctions for enhanced solar hydrogen generation. ***ACS Catal***, 2016, 6: 532–541.

[15] Masa J, Weide P, Peeters D, *et al.* Amorphous cobalt boride (Co_2B) as a highly efficient nonprecious catalyst for electrochemical water splitting: oxygen and hydrogen evolution[J]. ***Advanced Energy Materials***, 2016, 6(6): 1502313.

[16] Yu H, Chen W, Wang X, *et al.* Enhanced photocatalytic activity and photoinduced stability of Ag-based photocatalysts: the synergistic action of amorphous-Ti(IV) and Fe(III) cocatalysts. ***Applied Catalysis B: Environmental***, 2016, 187: 163-170.

[17] Liu J., Jia Q., Long J., *et al.* Amorphous NiO as co-catalyst for enhanced visible-light-driven hydrogen generation over g-C_3N_4 photocatalyst. ***Applied Catalysis B: Environmental***, 2018, 222: 35-43.

[18] Tran P. D., Tran T. V., Orio M., *et al.* Coordination polymer structure and revisited hydrogen evolution catalytic mechanism for amorphous molybdenum sulfide. ***Nature materials***, 2016, 15(6): 640.

[19] Qiao B., Wang A., Yang X., *et al.* Single-atom catalysis of CO oxidation using Pt_1/FeOx. ***Nature chemistry***, 2011, 3(8): 634.

[20] Yang M., Allard L. F., Flytzani-Stephanopoulos M. Atomically dispersed Au-(OH)x species bound on titania catalyze the low-temperature water-gas shift reactio. ***Journal of the American Chemical Society***, 2013, 135(10): 3768-3771.

[21] Kistamurthy D, Saib A M, Moodley D J, *et al.* Ostwald ripening on a planar Co/SiO_2 catalyst exposed to model Fischer–Tropsch synthesis conditions. ***Journal of catalysis***, 2015, 328: 123-129.

[22] Wang, R. Y., Wang, J. X., Jia, J., & Wu, H. S.. The growth pattern and electronic structures of Cu_n (n= 1-14) clusters on rutile TiO_2 (1 1 0) surface. ***Applied Surface Science***, 2021, 536, 147793.

[23] Mao, R., Kong, B. D., & Kim, K. W. . Thermal transport properties of metal/MoS_2 interfaces from first principles. ***Journal of Applied Physics***, 2014, 116(3), 034302.

[24] An X., Hu C., Liu H., *et al.* Hierarchical Nanotubular Anatase/Rutile/TiO_2(B) Heterophase Junction with Oxygen Vacancies for Enhanced Photocatalytic H_2 Production. ***Langmuir the Acs Journal of Surfaces & Colloids***, 2018, 34(5), 1883-1889.

[25] Wang, J., Guan, Z., Huang, J., Li, Q., & Yang, J.. Enhanced photocatalytic mechanism for the hybrid g-C_3N_4/MoS_2 nanocomposite. ***Journal of Materials Chemistry A***, 2014, 2(21), 7960-7966.

[26] J. Liu, Origin of high photocatalytic efficiency in monolayer g-C_3N_4/CdS heterostructure: A hybrid DFT study, ***J. Phys. Chem. C*** , 2015,119,28417-28423.

[27] Guo, L., Yang, Z., Marcus, K., Li, Z., Luo, B., & Zhou, L., *et al.*. MoS_2/TiO_2 heterostructures as nonmetal plasmonic photocatalysts for highly efficient hydrogen evolution. ***Energy & Environmental science***, 2017, 11(1), 106-114.

[28] Opoku, F., Govender, K. K., Sittert, C. V., & Govender, P. P.. Tuning the electronic structures, work functions, optical property and stability of bifunctional hybrid graphene oxide/v-doped $NaNbO_3$ type-Π heterostructures: a promising photocatalyst for H_2 production. ***Carbon***, 2018, 136, 187-195.

[29] Zhao, T., Chen, J., Wang, X., & Yao, M. Probing the electronic structure and photocatalytic performance of g-SiC/MoSSe van der Waals heterostructures: A first-principle study. ***Applied Surface Science***, 2021, 536, 147708.

[30] Wang, J., Guan, Z., Huang, J., Li, Q., & Yang, J.. Enhanced photocatalytic mechanism for the hybrid g-C_3N_4/MoS_2 nanocomposite. ***Journal of Materials Chemistry A***, 2014, 2(21), 7960-7966.

[31] Pearson, R. G.. Absolute electronegativity and absolute hardness of Lewis acids and bases. ***Journal of the American Chemical Society***, 1985, 107(24), 6801-6806.